

# Optimizing entanglement in two-qubit systems

Salvio Luna-Hernández<sup>1</sup>, Claudia Quintana<sup>2</sup>, and Oscar Rosas-Ortiz<sup>1,\*</sup>

<sup>1</sup>Physics Department, Cinvestav, AP 14-740, 07000 México City, Mexico

<sup>2</sup>School of Engineering and Sciences, Tecnológico de Monterrey, Atizapán 52926, Mexico

\*Correspondence: oscar.rosas@cinvestav.mx

## Abstract

We investigate entanglement in two-qubit systems using a geometric representation based on the minimum of essential parameters. The states are X-shaped and host pairs of identical populations while reducing the number of coherences involved. A geometric  $L$ -measure of entanglement is introduced as the distance between the points that represent entangled states and the closest point that defines separable states. Our results give a geometric meaning to the Hill-Wootters concurrence  $C$  since  $L$  coincides with  $C$ . Furthermore, unlike  $C$ , the measure  $L$  distinguishes the rank of states with maximum entanglement. We construct a time-dependent two-qubit state, traced out over the complementary components of a pure tetra-partite system, and find that its one-qubit states share the same entropy. The entanglement measure results bounded from above by the envelope of the minima of such entropy.

## 1 Main

Quantum correlations characterize the features of quantum multipartite systems that cannot be described by classical-like theories. Closely related to the concept of quantum coherence, no quantum correlation is viable without interference with respect to distinguishable alternatives of quantum states. Nowadays nonclassical correlations are invaluable resources for quantum information and quantum computation [1], but they emerged on the scene by raising one of the most important problems in the foundations of quantum theory [2, 3] and, surprisingly, by providing the solution of the same [4, 5]. Schrödinger introduced the expression *entanglement* for this first manifestation of quantum correlation [3]. The concept describes what occurs with our knowledge of two systems that are separated after they were interacting for a while, and from which we had maximal knowledge before the interaction [6]. In this sense, entanglement implies that the state of a composite system cannot be separated into the states of its parts. However, entanglement does not account for all quantum correlations, and even separable states may exhibit correlations that are not completely classical.

The entanglement in a system can be characterized and quantified from different points of view [7–13]. However, the separability criterion introduced by Peres [14] and Horodecki’s [15] provides a powerful tool for its detection. In this work, the Peres-Horodecki (also known as positive partial transpose –PPT–) criterion is applied to construct a convex representation of two-qubit states that permits the study of entanglement in purely geometric form. It is well known that this criterion is necessary and sufficient to detect entanglement in  $2 \otimes 2$  and  $2 \otimes 3$  quantum systems [15], so we will use it to identify entanglement in two-qubit mixed states. There are several incentives to consider these states, mainly because generating pure entangled states is not an easy task, so entangled states could be prepared as statistical mixtures for purely experimental reasons, but in general they can be the result of a partial trace of the quantum state of a larger system.

In general, mixed states characterize the interaction between the system and its environment, and the study of their entanglement properties is not only more complicated than that of pure states, but lesser understood. Although the first entangled system found in physics was in a pure state [2], it is in one of the Bell states [4], shortly after mixed states were identified that also disrupt the foundations of quantum theory [16]. These states, named after Werner, can be modeled using hidden variables without violating the Bell inequalities, and find applications in a diversity of quantum entanglement subjects [17–23]. Our results include a wide class of Werner states as a particular case.

We investigate the entanglement properties of two-qubit systems by using the minimum of essential parameters. The idea is to construct density operators whose reduced one-qubit states share the same entropy, regardless of whether the state of the entire system is pure or mixed. In this way, we identify X-shaped states [24–26], denoted  $\rho_X$ , that have the capacity to host pairs of identical populations while reducing the number of coherences involved. Demanding positive semidefinite, self-adjoint and normalized density operators  $\rho_X$ , and imposing the Peres-Horodecki criterion, we find a system of inequalities that related matrix elements must satisfy to determine both, the eligibility of  $\rho_X$  as a quantum state, and the possibility of finding entanglement. The solution of such a system defines a convex set  $\mathcal{S}$  that can be divided in subsets whose points define separable states and regions where entanglement may be found.

Based on the convex representation provided by  $\mathcal{S}$ , we introduce a geometric  $L$ -measure of entanglement, a distance-like entanglement measure [27], that coincides with the Hill-Wootters generalized concurrence  $C$  [28, 29] when applied to states  $\rho_X$ . Thus, our results give  $C$  a geometric meaning that is not obvious without the convex structure  $\mathcal{S}$ . Furthermore, unlike  $C$ , the measure  $L$  distinguishes the rank of states with maximum entanglement. The latter is relevant to determine not only the amount of quantum correlations but rather the quantumness of the state [30], so it shows how much useful a state is for a specific quantum processing task [31, 32]. Another advantage of the geometric  $L$ -measure is that, with respect to other entanglement measures, it allows comparatively easy calculation.

We also study what happens to entanglement when the system depends explicitly on time. Modeling an entangled diatomic system whose one-qubit parts are placed in inde-

pendent, isolated and identical electromagnetic cavities, each of which contains  $n$  photons, we construct a tetra-partite pure state that continues to evolve unitarily as a pure state. However, the reduced diatomic state does not evolve in a reversible way (systems like this may show signatures of chaos [33]), which makes it an excellent subject of study to understand the behavior of entanglement in systems described by time-dependent statistical mixtures. Regardless of the dynamical law obeyed by the time-dependent diatomic state, the corresponding one-qubit states share the same von Neumann entropy  $S$ , which oscillates as time passes. Our results verify that finding reduced states of maximum mixing does not provide information about the entanglement (if any) of the entire system when it is in a mixed state. However, the envelope formed by the minima of  $S$  defines an upper bound for the entanglement measurement. To the best of our knowledge, this remarkable result has gone unnoticed in the literature on the matter.

## 2 Two-qubit states

The density operator of any two-qubit system can be written as a  $4 \times 4$  complex matrix over the field  $\mathbb{C}$ ,

$$\rho = (r_{kj}), \quad r_{jk} = r_{kj}^* \in \mathbb{C}, \quad k, j \in \{1, 2, 3, 4\}, \quad \sum_{k=1}^4 r_{kk} = 1, \quad (1)$$

where  $z^*$  stands for the complex-conjugate of  $z \in \mathbb{C}$ . The populations (diagonal elements) and coherences (off-diagonal elements) are such that  $\rho$  is self-adjoint ( $\rho = \rho^\dagger$ ), normalized ( $\text{Tr } \rho = 1$ ) and positive semidefinite ( $\rho \geq 0$ ). The condition  $\text{Tr } \rho^2 = 1$  is necessary and sufficient for a density operator  $\rho$  to represent a pure state. In turn,  $\rho$  refers to mixed states if  $\text{Tr } \rho^2 < 1$ .

Hereafter, to represent states in the Hilbert space  $\mathcal{H} = \mathbb{C}^4$ , we use the computational basis  $|00\rangle \equiv |e_1\rangle$ ,  $|01\rangle \equiv |e_2\rangle$ ,  $|10\rangle \equiv |e_3\rangle$ ,  $|11\rangle \equiv |e_4\rangle$ , with  $|e_1\rangle = (1, 0, 0, 0)^T$ , and so on.

Assuming that the matrix-representation of  $\rho$  is known in advance, there is a simple way to identify whether or not it represents a pure state, which consists of the applicability of the following proposition (the proof is provided in Appendix A).

**Proposition Q.** If the matrix-elements of the two-qubit density operator  $\rho = (r_{kj})$  can be factorized in the form  $r_{kj} = \alpha_k \alpha_j^*$ , with  $\alpha_k, \alpha_j \in \mathbb{C}$ , and  $k, j \in \{1, 2, 3, 4\}$ , then  $\rho$  represents the pure state  $|\psi\rangle = \sum_{k=1}^4 \alpha_k |e_k\rangle$ .

We are interested in density operators whose matrix-elements do not necessarily satisfy Proposition Q, which opens the possibility of investigating entanglement in two-qubit mixed states. Among the diverse ways to prepare such states, we pay attention to the representation generated by the computational basis.

To outline the profile of the states of our interest, let us consider the reduced density operators  $\rho_{1,2} = \text{Tr}_{2,1} \rho$ . After diagonalizing, we obtain  $\rho_{k,\text{diag}} = \text{diag}(\lambda_k, 1 - \lambda_k)$ , where  $\lambda_k = (1 - \sqrt{1 - 4 \det \rho_k})/2$  is the smallest eigenvalue of  $\rho_k$ . The probability vectors

$\vec{\lambda}_k = (\lambda_k, 1 - \lambda_k)$  do not match in general since  $\det \rho_2 = \det \rho_1 + \Delta$ , with

$$\Delta = (r_{11} - r_{44})(r_{22} - r_{33}) + |r_{13} + r_{24}|^2 - |r_{12} + r_{34}|^2. \quad (2)$$

However, if  $\Delta = 0$  then  $\vec{\lambda}_1 = \vec{\lambda}_2 = \vec{\lambda} = (\lambda, 1 - \lambda)$  and  $\rho_{1,\text{diag}} = \rho_{2,\text{diag}}$ . Therefore, the von Neumann entropy gives the same result for both reduced matrices  $S(\rho_1) = S(\rho_2)$ .

Throughout this work the search for subsystems with equal entropy serves as a way to construct two-qubit mixed states that require a reduced number of parameters to characterize their possible entanglement. As long as we have these states, we will establish a mechanism to identify (and measure) entanglement.

With respect to the degree of mixing, the matrix rank of  $\rho$  (the number of its nonzero eigenvalues) is quite useful since it identifies the minimum number of pure states needed to prepare the corresponding statistical mixture. In fact, this notion is directly related to the purity of  $\rho$  since a pure state has rank 1 (and purity 1). So that purity less than 1 implies rank greater than 1.

A very simple form to satisfy  $\Delta = 0$  is by imposing the constraint

$$r_{13} = r_{24} = r_{12} = r_{34} = 0, \quad (3)$$

which yields diagonal reduced matrices, together with at least one of the following conditions

$$r_{11} = r_{44}, \quad r_{22} = r_{33}. \quad (4)$$

## 2.1 X-states

To construct states that satisfy the  $\Delta = 0$  requirement, let us first consider that only condition (3) is satisfied. In this case the density operators (1) are X-shaped,

$$\rho_X = \begin{pmatrix} r_{11} & 0 & 0 & r_{14} \\ 0 & r_{22} & r_{23} & 0 \\ 0 & r_{23}^* & r_{33} & 0 \\ r_{14}^* & 0 & 0 & r_{44} \end{pmatrix}. \quad (5)$$

Since coherence is a basis-dependent concept, states represented by non-diagonal density operators contain a certain amount of coherence with respect to the chosen basis. To be concrete, as density operators (1) are written in terms of the computational basis, their nonzero coherences  $r_{kj}$ ,  $k \neq j$ , determine the possibility of quantum interference with respect to the distinguishable alternatives  $|e_k\rangle$  and  $|e_j\rangle$ . In this way, for X-states (5), interference is only allowed between  $|e_1\rangle = |00\rangle$  and  $|e_4\rangle = |11\rangle$ , as well as between  $|e_2\rangle = |01\rangle$  and  $|e_3\rangle = |10\rangle$ . Any other interference between the elements of the basis is not allowed. In the most general case both interferences occur simultaneously, but entanglement arises when at least one of them is activated.

To analyze the properties of X-states as generally as possible, it is necessary to ensure that  $\rho_X$  is in fact a density operator. By construction,  $\rho_X$  is self-adjoint and normalized, so we just need to make sure that it is positive semidefinite.

After calculating the eigenvalues of  $\rho_X$ , see explicit expressions in Eq. (A-1) of Appendix A, we find that they are non-negative as long as the following conditions are met

$$|r_{14}| \leq \sqrt{r_{11}r_{44}}, \quad |r_{23}| \leq \sqrt{r_{22}r_{33}}. \quad (6)$$

That is,  $\rho_X$  represents an admissible quantum state, pure or mixed, only if the coherence amplitudes  $|r_{14}|$  and  $|r_{23}|$  are upper bounded by the population of the corresponding states.

### 2.1.1 Subsystems with equal entropy

Assuming that not only (3) but the first identity of Eq. (4) is also satisfied, states (5) will have the same population for states  $|e_1\rangle = |00\rangle$  and  $|e_4\rangle = |11\rangle$ . As a consequence, the reduced states will have the same probability vector  $\vec{\lambda}_L = (\lambda_L, 1 - \lambda_L)$ , with  $\lambda_L = (1 - |r_{22} - r_{33}|)/2$  and  $2r_{11} + r_{22} + r_{33} = 1$ . On the other hand, satisfying (3) and the second identity of Eq. (4) leads to states (5) characterized by having the same population for states  $|e_2\rangle = |01\rangle$  and  $|e_3\rangle = |10\rangle$ . The probability vector is now  $\vec{\lambda}_R = (\lambda_R, 1 - \lambda_R)$ , with  $\lambda_R = (1 - |r_{11} - r_{44}|)/2$  and  $r_{11} + 2r_{22} + r_{44} = 1$ . Since populations satisfy  $0 \leq r_{kk} \leq 1$ , we obtain  $0 \leq \lambda_{L,R} \leq \frac{1}{2}$ . That is, in general, neither of the two previous cases maximizes entropy.

Reduced matrices with maximal entropy are achieved if, in addition, we make  $r_{22} = r_{33}$  in  $\lambda_L$  and  $r_{11} = r_{44}$  in  $\lambda_R$ . The latter corresponds to also satisfying the complementary identity of Eq. (4) in each case. That is, only if (3) and both identities of Eq. (4) are satisfied, one gets  $\lambda_L = \lambda_R = 1/2$ .

In Appendix A we show that once Proposition Q is satisfied, applying the above conditions to state  $\rho_X$  leads to the Bell-states

$$|\beta_1\rangle = \frac{|e_1\rangle + |e_4\rangle}{\sqrt{2}}, \quad |\beta_2\rangle = \frac{|e_1\rangle - |e_4\rangle}{\sqrt{2}}, \quad (7)$$

and

$$|\beta_3\rangle = \frac{|e_2\rangle + |e_3\rangle}{\sqrt{2}}, \quad |\beta_4\rangle = \frac{|e_2\rangle - |e_3\rangle}{\sqrt{2}}. \quad (8)$$

To give an immediate, general example, consider the convex combination

$$\rho_B = \sum_{k=1}^4 b_k |\beta_k\rangle \langle \beta_k|, \quad 0 \leq b_k \leq 1, \quad \sum_{k=1}^4 b_k = 1. \quad (9)$$

This density operator is X-shaped and can accommodate two pairs of equally weighted populations. Namely,  $r_{11} = r_{44} = \frac{b_1 + b_2}{2}$  and  $r_{22} = r_{33} = \frac{b_3 + b_4}{2}$ , with  $r_{11} + r_{22} = \frac{1}{2}$ . The other non-zero matrix elements are  $r_{14} = r_{14}^* = \frac{b_1 - b_2}{2}$  and  $r_{23} = r_{23}^* = \frac{b_3 - b_4}{2}$ .

The one-qubit states that make up  $\rho_B$  are maximally mixed  $S(\rho_{B,1}) = S(\rho_{B,2}) = 1$ , regardless of  $r_{11}$  and  $r_{22}$ . This includes the extreme cases when  $\rho_B$  is either a Bell-state ( $b_k = 1$  for a given  $k$ ) or an equally weighted statistical mixture of Bell-states ( $b_k = \frac{1}{4}$  for any  $k$ ).

An interesting particular case of the previous model is achieved by setting  $b_k = (1 + 3q)/4$ , and  $b_j = (1 - q)/4$  for  $k = \text{fixed}$ , and  $j \neq k$ . This leads to the Werner-states [16]:

$$\rho_{W_k} = q|\beta_k\rangle\langle\beta_k| + \left(\frac{1-q}{4}\right)\mathbb{I}, \quad -\frac{1}{3} \leq q \leq 1, \quad k = 1, 2, 3, 4. \quad (10)$$

These states can be generalized to the configuration

$$\rho_S = \sum_{k=1}^4 q_k |\beta_k\rangle\langle\beta_k| + \left(\frac{1-s}{4}\right)\mathbb{I}, \quad \sum_{k=1}^4 q_k = s, \quad \frac{s-1}{4} \leq q_k \leq \frac{s+3}{4}, \quad (11)$$

where  $s \leq 1 + q_{\min}$  and  $q_{\min} = \min\{q_1, q_2, q_3, q_4\}$ . Note that  $\rho_S$  is another variation of  $\rho_B$ .

## 2.2 Entanglement conditions

The positive partial transposition of the density operator (1) obeys the following transformation rules

$$\rho^{T_1} : \quad r_{13} \rightarrow r_{13}^*, \quad r_{14} \rightarrow r_{23}^*, \quad r_{24} \rightarrow r_{24}^*.$$

$$\rho^{T_2} : \quad r_{12} \rightarrow r_{12}^*, \quad r_{14} \rightarrow r_{23}, \quad r_{34} \rightarrow r_{34}^*.$$

Without loss of generality, we will use the transposition with respect to the second qubit.

The transposition of the X-state (5) corresponds to make  $r_{14} \rightarrow r_{23}$ . Eigenvalues (A-1) and eigenvectors (A-2) must be transformed accordingly to solve the eigenvalue equation  $\rho_X^{T_2}|\tilde{e}\rangle = \tilde{\Lambda}|\tilde{e}\rangle$ . Then, it is found that  $\rho_X^{T_2}$  is positive semidefinite whenever  $|r_{23}| \leq \sqrt{r_{11}r_{44}}$  and  $|r_{14}| \leq \sqrt{r_{22}r_{33}}$ . Applying the Peres–Horodecki criterion [14, 15], we find that  $\rho_X$  is entangled as long as one of the following inequalities hold

$$|r_{23}| > \sqrt{r_{11}r_{44}}, \quad |r_{14}| > \sqrt{r_{22}r_{33}}. \quad (12)$$

This result imposes a lower limit on the coherence amplitudes that is unexpectedly determined by the populations of the complementary states. That is, to find entanglement,  $|r_{14}|$  must be lower bounded by the population of states  $|e_2\rangle = |01\rangle$  and  $|e_3\rangle = |10\rangle$ . Similar conclusions hold for the coherence amplitude  $|r_{23}|$  and populations  $r_{11}$  and  $r_{44}$ .

Thus, once the populations of the X-states are known, the coherences determine both the eligibility of  $\rho_X$  as a quantum state and the possibility of finding entanglement.

## 3 Convex optimization

To characterize entanglement in the X-states we have found a system of inequalities. Remember, (6) has been introduced to ensure that  $\rho_X$  is positive semidefinite while (12) obeys the Peres–Horodecki criterion for entanglement.

Using shorter notation we write  $x_0 = \sqrt{r_{11}r_{44}}$ ,  $y_0 = \sqrt{r_{22}r_{33}}$ ,  $r_{14} = xe^{i\theta}$  and  $r_{23} = ye^{i\phi}$ , with  $0 \leq \theta, \phi < 2\pi$ . In this way, condition (6) reads

$$0 \leq x \leq x_0, \quad 0 \leq y \leq y_0. \quad (13)$$

The combined inequalities (13) delimit a convex region of the  $xy$ -plane defined by  $0 \leq x + y \leq x_0 + y_0$ . The maximum value of the upper bound is optimized as  $(x_0 + y_0)_{\max} = 1/2$ , see details in Appendix A. Therefore,  $\rho_X$  is positive semidefinite for the points contained in the convex set

$$\mathcal{S} = \{(x, y) \in \mathbb{R}^2; 0 \leq x + y \leq \frac{1}{2}\}. \quad (14)$$

Geometrically,  $\mathcal{S}$  is nothing more than the right-triangle shown in Figure 1.

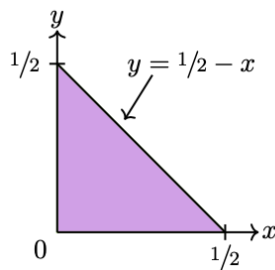


Figure 1: The points of the convex set  $\mathcal{S} \subset \mathbb{R}^2$ , a right-triangle with legs of length  $1/2$ , determine the matrix elements with which the density operator  $\rho_X$  becomes positive semidefinite.

This is the scenario where at least one of the inequalities (12) must be satisfied to obtain entanglement. We have two possible configurations,

$$0 \leq y \leq y_0, \quad y_0 < x \leq x_0, \quad (15)$$

or

$$0 \leq x \leq x_0, \quad x_0 < y \leq y_0. \quad (16)$$

Consider for example the Werner-states (10). If  $k = 1, 2$ , we find  $y = 0$ ,  $x = \frac{1}{2}|q|$ ,  $y_0 = \frac{1}{4}(1 - q)$  and  $x_0 = \frac{1}{4}(1 + q)$ , see Figure 2(a). To find entanglement,  $x$  must obey inequalities (15). If  $k = 3, 4$ , the results are obtained from the latter by changing  $x_0 \leftrightarrow y_0$  and  $x \leftrightarrow y$ , see Figure 2(b). Entanglement is now found whenever  $y$  obeys inequalities (16). The most striking thing about these results is that all states  $\rho_{W_k}$  share the same entanglement profile, they are entangled for  $q \in (1/3, 1]$ , regardless of  $k$ .

Note that  $\rho_{W_k}$  coincides with  $\rho_B$  if  $b_k = (3q + 1)/4$  and  $b_j = (1 - q)/4$ , where  $k = \text{fixed}$  and  $j \neq k$ . That is, the states  $\rho_{W_k}$  shown in Figure 2 correspond to concrete convex combinations of the four Bell-states, where  $|\beta_k\rangle$  plays a leading role.

To highlight the relevance of the Bell-states involved in any statistical mixture, let us analyze the (generalized) Werner-state (11) with only two non-zero  $q_k$  coefficients. If  $s \neq 1$ , this state also involves the four Bell-states. However, if  $s = 1$ , it is reduced to a statistical mixture of only two Bell-states, those involved with coefficients  $q_k \neq 0$ . The



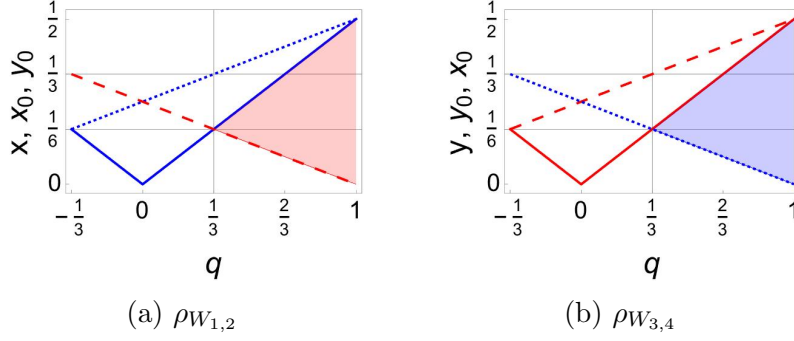


Figure 2: Entanglement conditions for the Werner-states  $\rho_{W_k}$ , with  $x = |r_{14}|$  (blue-continuous),  $y = |r_{23}|$  (red continuous),  $x_0 = \sqrt{r_{11}r_{44}}$  (blue-dotted), and  $y_0 = \sqrt{r_{22}r_{33}}$  (red-dashed). Two general cases are distinguished **(a)** If  $k = 1, 2$ , then  $y = 0$ . To find entanglement the coherence amplitude  $x$  must obey inequalities (15), see shaded-red area **(b)** If  $k = 3, 4$ , then  $x = 0$ . Entanglement is found whenever the coherence amplitude  $y$  obeys inequalities (16), see shaded-blue area.

model is illustrated in Figure 3 with  $b_k = q$ ,  $b_j = 1 - q$ , and  $q_k = q$ ,  $q_j = s - q$ , for  $\rho_B$  and  $\rho_S$  respectively. In all cases  $k$  and  $j \neq k$  are fixed. As in the previous case, what is common in all the states shown in Figure 3 is their entanglement profile.

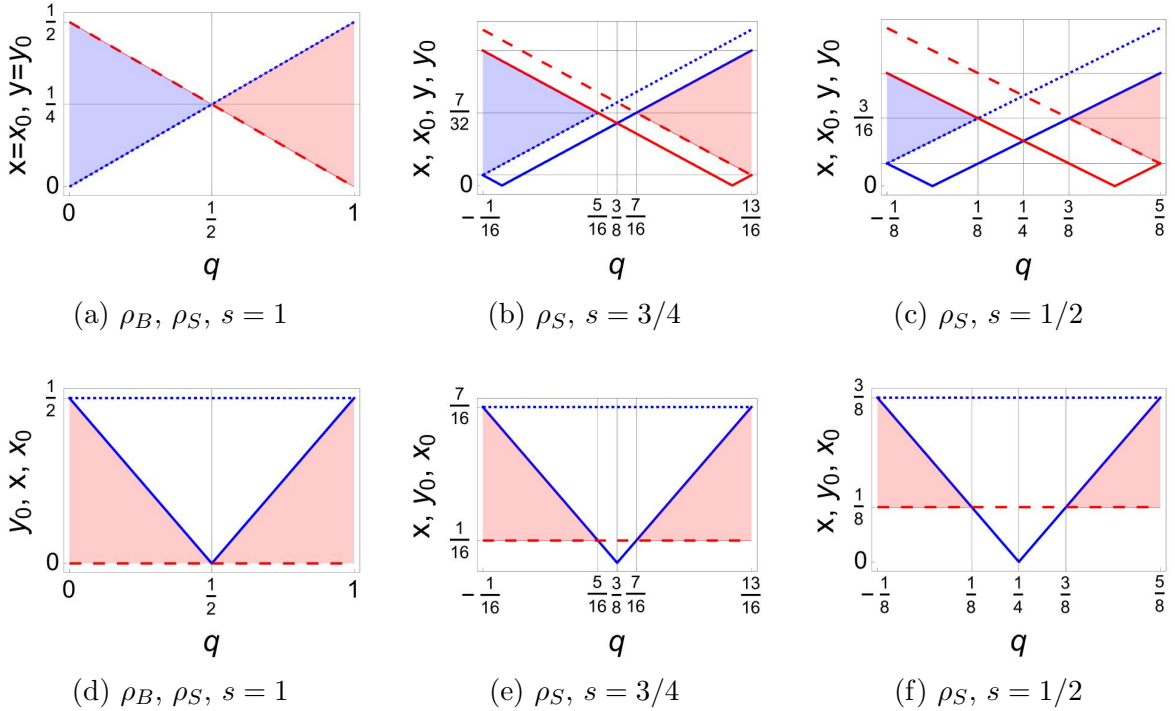


Figure 3: Entanglement conditions for the statistical mixture of Bell-states  $\rho_B$  and the generalized Werner-state  $\rho_S$ , with only two nonzero coefficients  $b_k = q$ ,  $b_j = 1 - q$ , and  $q_k = q$ ,  $q_j = s - q$ , respectively. In all cases  $k$  and  $j \neq k$  are fixed. The **first row** refers to any pair  $(k, j)$ , except  $(1, 2)$  and  $(3, 4)$ . The **second row** illustrates the case  $(1, 2)$ , for which  $y = 0$ . The case  $(3, 4)$  is obtained from the second row after the changes  $x_0 \leftrightarrow y_0$ ,  $x \leftrightarrow y$ . Color code follows the instructions in Figure 2.



### 3.1 Entanglement

In what follows we assume that  $x_0$  and  $y_0$  are known in advance. The description in terms of the point  $p = (x, y) \in \mathcal{S}$  corresponds to determining the possible entanglement with respect to the coherences  $r_{14}$  and  $r_{23}$ .

The convex set  $\mathcal{S}$  can be divided into regions (subsets) whose points define separable states and regions where entanglement may be found. We distinguish three main classes, described below.

- Region  $\mathcal{M}_0$ . No entanglement is allowed if  $r_{11}r_{44} = r_{22}r_{33} \neq 0$ . That is, none of inequalities (15)-(16) apply if  $x_0 = y_0 \neq 0$ . Instead we have  $0 \leq x, y \leq x_0$ , so we have a square  $\square_{x_0}$  of sides  $x_0$ , with  $x_{0\max} = 1/4$ , see Figure 4. These points produce separable mixed states  $\rho_X$  that can be identified by their rank. According to the eigenvalues (A-1), the vertex  $q_\star = (x_0, x_0)$  represents rank-2 states. In turn,  $(x_0, y)$  and  $(x, y_0)$ , located respectively along the right-vertical and top sides of the square, define rank-3 states. Any other point of  $\square_{x_0}$  gives rank-4 states.

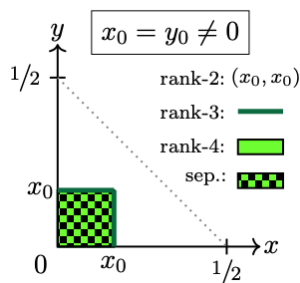


Figure 4: There is **no entanglement** if the populations of  $\rho_X$  satisfy  $r_{11}r_{44} = r_{22}r_{33} \neq 0$ . In notation of the convex set  $\mathcal{S}$ , the latter means  $x_0 = y_0 \neq 0$ . The points  $(x, y) \in \mathcal{S}$  that meet this condition form a square  $\square_{x_0}$  of sides  $x_0$ , with  $x_{0\max} = 1/4$ .

As an example consider the states  $\rho_B = \rho_S$  shown in Figure 3(a). Entanglement is lost precisely at  $q = 1/2$ , where  $x_0 = y_0 = 1/4$  puts vertex  $q_\star = (x_0, x_0)$  to the middle of the hypotenuse of  $\mathcal{S}$ . The same is true for the states  $\rho_{W_k}$  exhibited in Figure 2, at  $q = 0$ .

- Region  $\mathcal{M}_1$ . To satisfy inequalities (15) it is necessary to take the ordering  $0 \leq y_0 < x_0$ , see for example the shaded-red area in Figures 2 and 3. The entanglement set is a rectangle lying on the horizontal leg of  $\mathcal{S}$ , as shown in Figure 5(a). The square  $\square_{y_0}$  of separable states is located just to the left of such rectangle.

Using the eigenvalues (A-1) we find that vertex  $q_0 = (x_0, y_0)$  gives rank-2 states. Points along the right-vertical side and the top of the rectangle,  $(x_0, y)$  and  $(x, y_0)$  respectively, yield rank-3 states. Any other point of this entanglement set provides rank-4 states.

A very important subset  $\mathcal{M}_x \subset \mathcal{M}_1$ , defined by the coherence amplitudes  $y = 0$  (regardless of  $y_0$ ), provides points restricted to the horizontal leg of  $\mathcal{S}$ . Hereafter, the states defined by points  $(x, 0) \in \mathcal{M}_x$  will be denoted by  $\rho_{\mathcal{M}_x}$ . Since  $y = 0$ , to find entanglement, our interest is addressed to the coherence amplitudes  $x$  that satisfy  $y_0 < x \leq x_0$ . As an

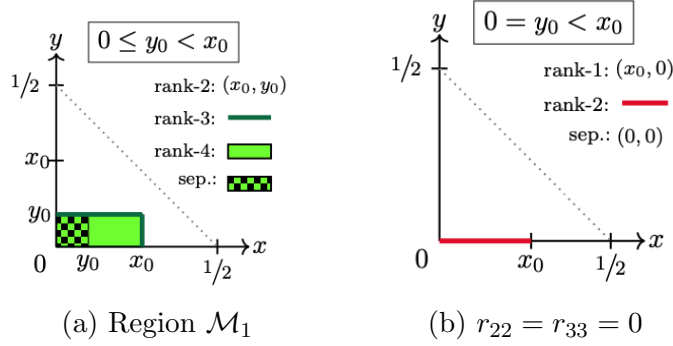


Figure 5: Entanglement conditions for states  $\rho_{\mathcal{M}_1}$ ; the entanglement set is shaded-green, the chessboard region corresponds to separable states (a) According to (15), entanglement is encoded in a rectangle with base  $x_0 - y_0$  and height  $y_0$ . The square  $\square_{y_0}$  defines separable states (b) Setting  $y = y_0 = 0$ , with  $r_{22} = r_{33} = 0$ , the states  $\rho_{\mathcal{M}_x}$  acquire the form of the third matrix in Eq. (17), which is of rank-2 if  $x < x_0$ . The pure (rank-1) states  $|\psi_{14}\rangle$  are achieved if  $x = x_0$ , which includes the Bell-states  $|\beta_{1,2}\rangle$  when  $x = x_{0\max} = 1/2$

example consider the Werner-states  $\rho_{W_{1,2}}$  illustrated in Figure 2(a), as well as states  $\rho_S$  shown in the second row of Figure 3.

In general, by extending the domain of  $x$  to the maximum we optimize the entanglement in  $\mathcal{M}_x$ . For this, it is enough to set  $y_0 = 0$ . We find three different states

$$\begin{pmatrix} r_{11} & 0 & 0 & xe^{i\theta} \\ 0 & 0 & 0 & 0 \\ 0 & 0 & r_{33} & 0 \\ xe^{-i\theta} & 0 & 0 & r_{44} \end{pmatrix}, \quad \begin{pmatrix} r_{11} & 0 & 0 & xe^{i\theta} \\ 0 & r_{22} & 0 & 0 \\ 0 & 0 & 0 & 0 \\ xe^{-i\theta} & 0 & 0 & r_{44} \end{pmatrix}, \quad \begin{pmatrix} r_{11} & 0 & 0 & xe^{i\theta} \\ 0 & 0 & 0 & 0 \\ 0 & 0 & 0 & 0 \\ xe^{-i\theta} & 0 & 0 & r_{44} \end{pmatrix}. \quad (17)$$

Neither of the first two matrices in (17) satisfy the factorization of their elements as required in Proposition Q, so they represent mixed states of rank-3 or rank-2, see Eq. (A-6). In turn, if the elements of the third matrix are factorized we have  $x = x_0 = |\alpha_1\alpha_4|$ , so it represents the pure (rank-1) state  $|\psi_{14}\rangle$  defined in (A-3). In particular, if  $x = x_{0\max} = 1/2$  we recover the Bell-states  $|\beta_1\rangle$  and  $|\beta_2\rangle$ . If their elements cannot be factorized, this matrix represents a mixed state of rank-2, see Figure 5(b).

- Region  $\mathcal{M}_2$ . Inequalities (16) are satisfied by imposing the ordering  $0 \leq x_0 < y_0$ , see for example the shaded-blue area in Figures 2 and 3. The entanglement subset is also a rectangle, but in this case the base is placed just above the separable-states square  $\square_{x_0}$ , see Figure 6(a). Points along the right-vertical side and the top of the rectangle, respectively  $(x_0, y)$  and  $(x, y_0)$ , give rise to rank-3 states. In turn, vertex  $q_0 = (x_0, y_0)$  corresponds to rank-2 states. Any other point provides rank-4 states.

In this case the subset  $\mathcal{M}_y \subset \mathcal{M}_2$ , defined by the coherence amplitudes  $x = 0$ , provides points restricted to the vertical leg of  $\mathcal{S}$  and defines states  $\rho_{\mathcal{M}_y}$ . Our interest now turns to the region  $x_0 < y \leq y_0$ . As an example consider the Werner-states  $\rho_{W_{3,4}}$  exhibited in Figure 2(b) and the  $y$ -version of the states  $\rho_S$  shown in the second row of Figure 3. The

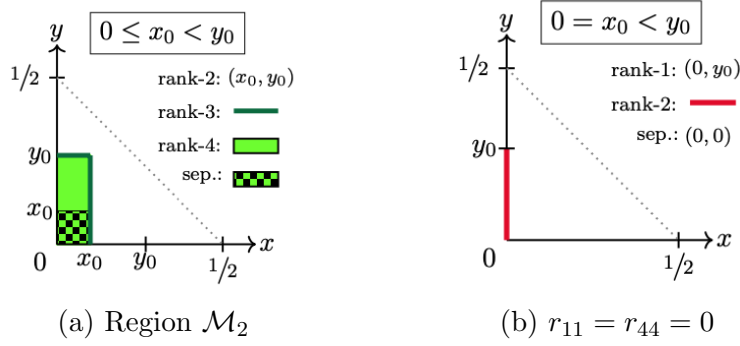


Figure 6: Entanglement conditions for states  $\rho_{\mathcal{M}_2}$  (a) According to (16), we find entanglement in a rectangle of base  $x_0$  and height  $y_0 - x_0$ . The square  $\square_{x_0}$  gives separable states (b) If  $x = x_0 = 0$ , with  $r_{11} = r_{44} = 0$ , the states  $\rho_{\mathcal{M}_y}$  acquire the form of the third matrix in Eq. (18), which is of rank-2 if  $y < y_0$ . The pure (rank-1) states  $|\psi_{23}\rangle$  are achieved if  $y = y_0$ , which includes the Bell-states  $|\beta_{3,4}\rangle$  when  $y = y_{0\max} = 1/2$ .

optimization is achieved by setting  $x_0 = 0$ , which results in the following states

$$\begin{pmatrix} 0 & 0 & 0 & 0 \\ 0 & r_{22} & ye^{i\phi} & 0 \\ 0 & ye^{-i\phi} & r_{33} & 0 \\ 0 & 0 & 0 & r_{44} \end{pmatrix}, \begin{pmatrix} r_{11} & 0 & 0 & 0 \\ 0 & r_{22} & ye^{i\phi} & 0 \\ 0 & ye^{-i\phi} & r_{33} & 0 \\ 0 & 0 & 0 & 0 \end{pmatrix}, \begin{pmatrix} 0 & 0 & 0 & 0 \\ 0 & r_{22} & ye^{i\phi} & 0 \\ 0 & ye^{-i\phi} & r_{33} & 0 \\ 0 & 0 & 0 & 0 \end{pmatrix}. \quad (18)$$

The first two matrices do not satisfy Proposition Q, so they represent mixed states of rank-3 or rank-2, see Eq. (A-7). If the elements of the third matrix are factorized we have  $y = y_0 = |\alpha_2\alpha_3|$ , so it represents the pure (rank-1) state  $|\psi_{23}\rangle$  defined in (A-4). If  $y = y_{0\max} = 1/2$ , we recover the Bell-states  $|\beta_3\rangle$  and  $|\beta_4\rangle$ . If their elements cannot be factorized, this matrix is a mixed state of rank-2, see Figure 6(b).

The classification developed above is very close to the parametrization of two-qubit X-density matrices with a fixed rank reported in Section 2.1 of [26]. The latter, based on the coefficients that define the characteristic equation for the density operator, considers the Newton-Girard formulae [34] and a very concrete parametrization of the matrix-elements of  $\rho_X$ . Beyond using the computational basis, our treatment is free of parametrization for the matrix elements  $r_{jk}$ , so it aims to be more practical and, therefore, universal. Nevertheless, the parameters used in [26] are very valuable as they comprise the information needed to obtain a unitary transformation that converts arbitrary two-qubit states into their X counterparts.

### 3.2 Geometric $L$ -measure

In the previous sections we have identified the regions of the convex set  $\mathcal{S}$  whose points would imply entanglement in state  $\rho_X$ . We know, for example, that squares  $\square_{x_0}$  and  $\square_{y_0}$  must be discarded because all their points represent separable states. However, we have not quantified the amount of entanglement that distinguishes some points from others in

any other region, nor have we analyzed which region offers better entanglement conditions. To address these points we proceed as follows.

We seek to ensure that entangled states “resemble” separable states as little as possible. Translated into the language of the convex set  $\mathcal{S}$ , this statement means that if  $p$  encodes entanglement then it should be as far away as possible from  $\square_{x_0}$  and  $\square_{y_0}$ . The further remote, the greater the entanglement. With this in mind, consider the metric  $d(\vec{r}_1, \vec{r}_2) = \max\{|x_2 - x_1|, |y_2 - y_1|\}$ , where  $\vec{r}_k = (x_k, y_k) \in \mathbb{R}^2$ ,  $k = 1, 2$ . We now introduce a geometric measure of entanglement for two-qubit systems.

**Definition.** (*L*-measure of entanglement) Given the extreme points  $x_0$  and  $y_0$ , let  $\mathcal{S}$  be the convex set (14) and  $\square_{z_0} \subset \mathcal{S}$  be the subset of points defining separable states. The *L*-measure of entanglement, applied to the point  $p \in \mathcal{S}$ , is the distance between  $p$  and the closest point  $q \in \square_{z_0}$  given by

$$L = \xi_0 \inf_q d(q, p),$$

with  $\xi_0$  a normalization factor.

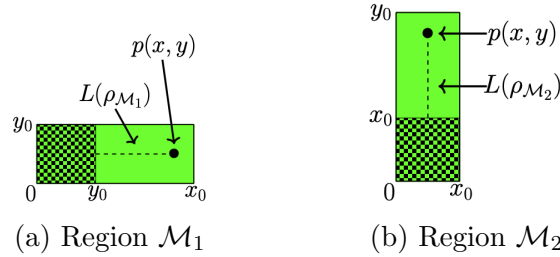


Figure 7: Illustration of the geometric notion of distance used to define the measure  $L$  for states  $\rho_X$  defined by points in regions  $\mathcal{M}_1$  or  $\mathcal{M}_2$ .

Let us apply the measure  $L$  to the points  $p \in \mathcal{S}$  that define the states classified in the previous section. States  $\rho_{\mathcal{M}_1}$  are such that  $\inf d(q, p)$  is given by the points  $q = (y_0, y)$ , see Figure 7(a). Therefore

$$L(\rho_{\mathcal{M}_1})|_{q=(y_0, y)} = 2 \max\{0, x - y_0\} = \begin{cases} 0 & \text{if } x < y_0 \\ 2(x - y_0) & \text{if } x > y_0 \end{cases} \quad (19)$$

Note that  $x = x_0$  defines the furthest point from the zone of separable states, therefore  $L_{\max}(\rho_{\mathcal{M}_1}) = 2(x_0 - y_0)$ . That is, among these states, the highest value of the *L*-measure is provided by the rank-3 states associated with the points  $(x_0, y)$ .

For states  $\rho_{\mathcal{M}_2}$  we find that  $q = (x, x_0)$  defines  $\inf d(q, p)$ , see Figure 7(b). Then

$$L(\rho_{\mathcal{M}_2})|_{q=(x, x_0)} = 2 \max\{0, y - x_0\} = \begin{cases} 0 & \text{if } y < x_0 \\ 2(y - x_0) & \text{if } y > x_0 \end{cases} \quad (20)$$

In this case the highest value of the *L*-measure is provided by the rank-3 states associated with the points  $(x, y_0)$ , so that  $L_{\max}(\rho_{\mathcal{M}_2}) = 2(y_0 - x_0)$ .

Combining the previous results we obtain the general rule

$$\begin{aligned} L(\rho_X) &= 2 \max \{0, x - y_0, y - x_0\} \\ &= 2 \max \left\{ 0, |r_{14}| - \sqrt{r_{22}r_{33}}, |r_{23}| - \sqrt{r_{11}r_{44}} \right\}. \end{aligned} \quad (21)$$

To find entanglement it is enough for one of the subtractions of (21) to be positive.

If  $x$  and  $y$  take the maximum value in their respective domains we have

$$L_{\max}(\rho_X) = 2 \max \{0, x_0 - y_0, y_0 - x_0\} = 2|x_0 - y_0| = 2|\sqrt{r_{11}r_{44}} - \sqrt{r_{22}r_{33}}|.$$

That is, when  $x_0$  and  $y_0$  are nonzero and different from each other, the strongest entanglement is exhibited by rank-3 states  $\rho_X$ . On the other hand, if  $x_0 = 0$  or  $y_0 = 0$ , the  $L$ -measure identifies rank-1 (pure) states as those with greater entanglement. In particular, if  $x_0 = x_{0\max} = 1/2$  or  $y_0 = y_{0\max} = 1/2$ , such states are not only pure but coincide with one of the Bell-states.

The most notable of the previous results is that the mathematical expression of the geometric measure  $L$  coincides precisely with the Hill-Wootters concurrence calculated for the  $\rho_X$  states. In fact, according with [28, 29], the concurrence for any state  $\rho$  is given by  $C(\rho) = \max\{0, \sqrt{\ell_1} - \sqrt{\ell_2} - \sqrt{\ell_3} - \sqrt{\ell_4}\}$ . The  $\ell_k$ 's are the eigenvalues (in decreasing order) of the matrix  $R_\rho = \rho(\sigma_2 \otimes \sigma_2)\rho^*(\sigma_2 \otimes \sigma_2)$ , with  $\sigma_2$  the well-known anti-diagonal Pauli-matrix.

Using state  $\rho_X$  to construct  $R_\rho$ , a simple calculation produces the eigenvalues  $(x_0 \pm x)^2$  and  $(y_0 \pm y)^2$ , where no order has yet been established. From (13) we know that the quantities in parentheses are not negative, so we have two different ways of sorting  $\sqrt{\ell_k}$  in descending order, with  $y_0 + y$  or  $x_0 + x$  leading. A little algebra produces the result

$$C(\rho_X) = \begin{cases} 2 \max \{0, y - x_0\}, & y_0 + y > x_0 + x \\ 2 \max \{0, x - y_0\}, & x_0 + x > y_0 + y \end{cases}$$

which once summarized leads to the identity  $C(\rho_X) = L(\rho_X)$ .

That is, the Hill-Wootters concurrence coincides with our  $L$ -measure when applied to state  $\rho_X$ . With this result we have given  $C(\rho_X)$  a geometric meaning that is not obvious without the structure of the convex set  $\mathcal{S}$ . What is even better is that, unlike concurrence, the geometric measure distinguishes the rank of states with maximum entanglement.

Once we have proven the identity  $C = L$ , it is appropriate to construct a geometric version of the entanglement of formation [35]. Following [29] we obtain

$$\varepsilon(\rho_{\mathcal{M}_1}) = \begin{cases} 0 & \text{if } x < y_0 \\ h\left(\frac{1 + \sqrt{1 - 4(x - y_0)^2}}{2}\right) & \text{if } x > y_0 \end{cases} \quad (22)$$

and

$$\varepsilon(\rho_{\mathcal{M}_2}) = \begin{cases} 0 & \text{if } y < x_0 \\ h\left(\frac{1 + \sqrt{1 - 4(y - x_0)^2}}{2}\right) & \text{if } y > x_0 \end{cases} \quad (23)$$

where  $h(z) = -z \log_2 z - (1 - z) \log_2(1 - z)$  is the Sahnnon binary entropy function.

### 3.3 Determination of entanglement

The entanglement of the Werner-states  $\rho_{W_k}$ , quantified by  $L$  and  $\varepsilon$ , is shown in Figure 8(a) (see also Figure 2). The optimization is achieved in half of the domain of  $q$  only.

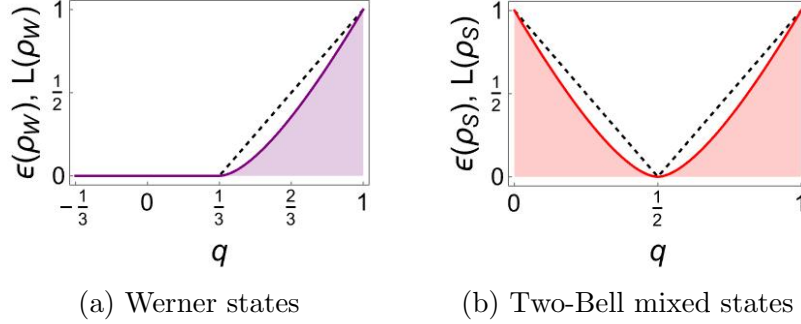


Figure 8: The geometric measure  $L$  (continuous curve) and entanglement of formation  $\varepsilon$  (dotted curve) applied to (a) the Werner-states  $\rho_{W_k}$  and (b) the statistical mixture  $\rho_B$  of only two Bell-states. There is no entanglement for half the domain of  $q$  in  $\rho_{W_k}$ , compare with Figure 2. In turn, states  $\rho_B$  lack entanglement only at one point ( $q = 1/2$ ) of the corresponding domain, compare with Figures 3(a) and 3(d).

Figure 8(b) shows the result of applying  $L$  and  $\varepsilon$  to the convex combinations of Bell-states exhibited in Figures 3(a) and 3(d). This time the optimization is over almost the entire domain of  $q$ , mainly in the neighborhoods of  $q = 0$  and  $q = 1$ , which serve as accumulation points. These systems are separable only for  $q = 1/2$ .

On the other hand, applying  $L$  and  $\varepsilon$  to the generalized Werner-states shown in Figure 3 produces results that depend on  $s$ , as expected. In Figure 9 we see that the maximum of  $L$  and  $\varepsilon$  decreases with  $s < 1$ . Furthermore, the interval of  $q$  for which  $L$  is equal to zero becomes increasingly larger. Thus, any perturbation that modifies the original statistical mixture (i.e., the value  $s = 1$ ) drastically affects entanglement: as mixing is maximized, the system loses quantum properties, making it increasingly classical.

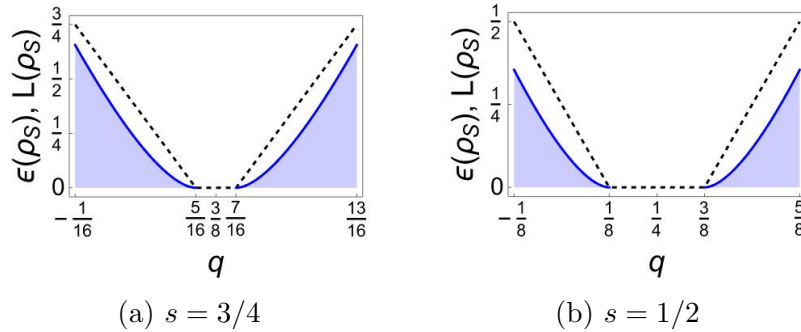


Figure 9: The geometric measure  $L$  (continuous curve) and entanglement of formation  $\varepsilon$  (dotted curve) applied to the generalized Werner-states shown in Figure 3. The case depicted in Figure 8(b) is recovered if  $s = 1$ . In general, the maximum values of  $L$  and  $\varepsilon$  decrease with  $s$  while the region where they become zero increases.

To further extend the applicability of our treatment, we now study what happens to entanglement when the system is explicitly time-dependent.

Suppose we have at hand a pair of two-level atoms which are entangled in energy, say  $|\psi_{2\text{at}}\rangle = |\beta_3\rangle$ . Let us place these atoms in independent, isolated and identical electromagnetic cavities, each of which containing exactly  $n$  photons. The state of the entire system can be written as  $|\Phi\rangle = \frac{1}{\sqrt{2}}(|+, n\rangle \otimes |-, n\rangle + |-, n\rangle \otimes |+, n\rangle)$ , where  $|n\rangle$  represents the state of the quantized field contained in each cavity. Besides  $|+\rangle \equiv |0\rangle$  and  $|-\rangle \equiv |1\rangle$ . Following [36–38], with  $\gamma$  a coupling factor, the time-evolved state acquires the form

$$\begin{aligned} |\Phi(t)\rangle &= \cos(\gamma t\sqrt{n+1}) [\cos(\gamma t\sqrt{n})|\varphi_1\rangle - i \sin(\gamma t\sqrt{n})|\varphi_2\rangle] \\ &\quad - i \sin(\gamma t\sqrt{n+1}) [\cos(\gamma t\sqrt{n})|\varphi_3\rangle - i \sin(\gamma t\sqrt{n})|\varphi_4\rangle], \end{aligned}$$

with  $|\varphi_1\rangle = |\Phi\rangle_{t=0}$ , and

$$\begin{aligned} |\varphi_2\rangle &= \frac{1}{\sqrt{2}}(|+, n\rangle \otimes |+, n-1\rangle + |+, n-1\rangle \otimes |+, n\rangle), \\ |\varphi_3\rangle &= \frac{1}{\sqrt{2}}(|-, n+1\rangle \otimes |-, n\rangle + |-, n\rangle \otimes |-, n+1\rangle), \\ |\varphi_4\rangle &= \frac{1}{\sqrt{2}}(|-, n+1\rangle \otimes |+, n-1\rangle + |+, n-1\rangle \otimes |-, n+1\rangle). \end{aligned}$$

The reduced time-dependent diatomic state results

$$\rho_{2\text{at}}(t) = \text{Tr}_{\text{fields}} \rho(t) = \begin{pmatrix} r_{11}(t) & 0 & 0 & 0 \\ 0 & y_0(t) & y(t) & 0 \\ 0 & y(t) & y_0(t) & 0 \\ 0 & 0 & 0 & r_{44}(t) \end{pmatrix}, \quad (24)$$

where

$$y_0(t) = \frac{1}{2} \cos^2(\gamma t\sqrt{n+1}) \cos^2(\gamma t\sqrt{n}) + \frac{1}{2} \sin^2(\gamma t\sqrt{n+1}) \sin^2(\gamma t\sqrt{n})$$

and

$$y(t) = \frac{1}{2} \cos^2(\gamma t\sqrt{n+1}) \cos^2(\gamma t\sqrt{n}).$$

In turn, the extreme point  $x_0 = \sqrt{r_{11}r_{44}}$  is obtained from the matrix-elements

$$r_{11}(t) = \cos^2(\gamma t\sqrt{n+1}) \sin^2(\gamma t\sqrt{n}), \quad r_{44}(t) = \sin^2(\gamma t\sqrt{n+1}) \cos^2(\gamma t\sqrt{n}).$$

The profile of the diatomic state  $\rho_{2\text{at}}$  fits the structure of  $\rho_{\mathcal{M}_y}$  at any time. The  $L$ -measure returns the value 1 at  $t = 0$ , where the diatomic system is in the Bell-state  $|\beta_3\rangle$ . As time passes,  $L$  decreases to zero and then increases until it is almost equal to 1. This process is repeated over and over again, see Figure 10(a). The time intervals where entanglement is zero coincide with the violation of inequality  $x_0 < y$ , see Figure 10(b).

We now focus our attention on the reduced states of  $\rho_{2\text{at}}$ , which have the same entropy  $S(\rho_1) = S(\rho_2)$ . In Figure 11 we have depicted the result of applying  $L$  and  $\varepsilon$  to  $\rho_{2\text{at}}$ ,



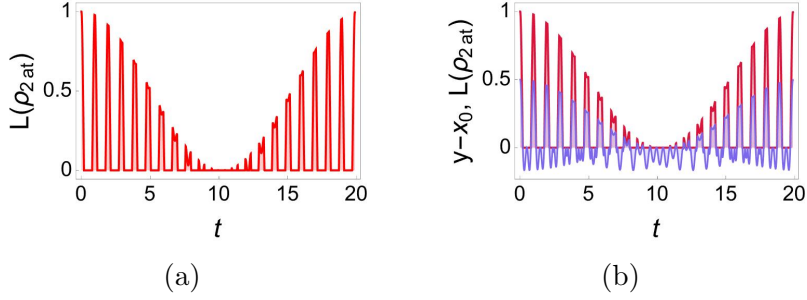


Figure 10: **(a)** The geometric measure  $L$  applied to the time-dependent diatomic state  $\rho_{2\text{at}}$ . As time passes,  $L$  decreases from 1 to zero and then increases until it is almost equal to 1. This process is repeated over and over again **(b)** Comparison of  $L(\rho_{2\text{at}})$  with the difference  $y - x_0$ . Clearly, inequality  $y > x_0$  is violated in the same time intervals where  $L = 0$ .

together with the entropy  $S(\rho_{1,2})$ . We see that  $S$  reaches its maximum value at different times. Some of such moments define also the local maxima of  $L$  and  $\varepsilon$ , but others are in time intervals where there is no entanglement. As it is well known, the latter means that finding reduced states of maximum mixing does not provide information about the entanglement (if any) of the entire system if it is in a mixed state. However, the minima of  $S$  play a different role in the system we are dealing with.

The envelope formed by the minima of  $S$  establishes an upper limit for the entanglement measurement. To our knowledge, this surprising property of entropy shared by reduced states has not been observed in the literature on the matter.

The phenomenon described above is also present when we use any other Bell-state as initial condition instead of  $|\beta_3\rangle$ . If we start from  $|\beta_4\rangle$  the structure of  $\rho_{2\text{at}}$  is similar to the one we find in (24). But starting from  $|\beta_{1,2}\rangle$  we arrive at a diatomic state of the form  $\rho_{\mathcal{M}_x}$ . In any case, what we find is that the envelope formed by the minima of  $S$  represents an upper bound on the entanglement strength as time progresses.

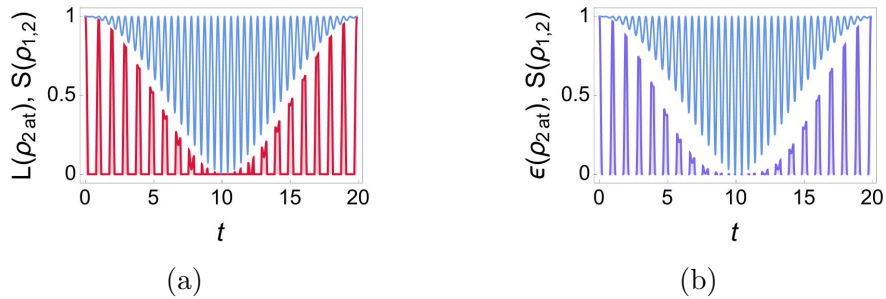


Figure 11: The envelope formed by the minima of the one-qubit entropy (blue curve) defines an upper bound for entanglement in the time-dependent diatomic state  $\rho_{2\text{at}}$  **(a)** The geometric measure  $L$  is red-shaded **(b)** The entanglement of formation  $\varepsilon$  is purple-shaded.

## 4 Conclusions

We have established the necessary conditions to study entanglement in two-qubit systems by using the minimum of essential parameters.

The idea has been to construct density operators whose reduced one-qubit states share the same entropy, regardless of whether the state of the entire system is pure or mixed. The latter leads to the identification of  $\rho_X$  states that have the capacity to host pairs of identical populations while reducing the number of coherences involved.

With the above results we have constructed a convex representation that facilitates the study of entanglement in two-qubit systems. The description is purely geometric and is based on two of the most striking results we have found:

i) To obtain positive semidefinite operators  $\rho_X$ , the coherence amplitudes  $x = |r_{14}|$  and  $y = |r_{23}|$  should be bounded from above by the corresponding populations,  $x_0 = \sqrt{r_{11}r_{44}}$  and  $y_0 = \sqrt{r_{22}r_{33}}$ . Otherwise,  $\rho_X$  is not a quantum state.

ii) To find entanglement,  $x$  and  $y$  should be bounded from below by the complementary populations,  $y_0$  and  $x_0$ , respectively. Otherwise, state  $\rho_X$  is separable.

Taking full advantage of such representation we have introduced a geometric measure  $L$ , which is defined as the distance between  $p$  (the point under study) and the closest point  $q$  that defines separable states. The more remote, the greater the entanglement.

The  $L$ -measure coincides with the Hill–Wootters generalized concurrence  $C$  for states  $\rho_X$ . That is, our results give  $C$  a geometric meaning that is not obvious without the convex structure introduced in this work. What is even better is that, unlike  $C$ , the geometric measure  $L$  distinguishes the rank of states with maximum entanglement.

We have found that rank-3 states  $\rho_X$  exhibit the strongest entanglement when  $x_0$  and  $y_0$  are nonzero and different from each other. These states have no locally producible quantum correlations since no rank-3 or rank-4 state can be produced by local operations of one of the parties on a classically correlated state [30,32]. If  $x_0 = 0$  and  $y = y_0$ , or  $y_0 = 0$  and  $x = x_0$ , states  $\rho_X$  are pure (rank-1) and yield strong entanglement. The Bell-states fall into this category by maximizing to 1 the result given by the measure  $L$ . It seems that states of higher ranks are more useful for quantum information procedures [32]. In particular, states of rank-3 can be used to reconstruct pure states by a remote party [31]. In turn, rank-4 states (which inhabit the different entanglement regions of  $\mathcal{S}$ ) are useful for reconstructing arbitrary states [32].

The applicability of our method goes far beyond the time-independent systems typically discussed in the literature. We have also studied what happens to entanglement when the system depends explicitly on time. Within the geometric representation, the time-evolution of  $\rho_X$  describes paths that transit between areas with different entanglement strength, even invading regions where the state becomes separable to return to the entanglement zones, and so on. The latter opens the possibility of manipulating and controlling entanglement in two-qubit systems by using inverse problem techniques [13,39].

We have found another outstanding result for the time-dependent system studied here. The envelope formed by the minima of  $S$ , the entropy of the reduced states, establishes an upper bound for the entanglement measurement. To our knowledge, this surprising property has not been reported in the literature on the matter.

## A

**Proposition Q** (proof). Let us write the density operator in the form  $\rho = \sum_{k,j=1}^4 r_{kj} \Gamma^{kj}$ , where the dyadic operators  $\Gamma^{kj} = |e_k\rangle\langle e_j|$ ,  $k, j \in \{1, 2, 3, 4\}$ , correspond to 4-square matrices for which all the entries are zero except the one in the  $k$ th row and the  $j$ th column, which acquires the value 1 [40]. These operators obey the multiplication rule  $\Gamma^{ij}\Gamma^{km} = \delta_{jk}\Gamma^{im}$ , and have the properties  $\sum_{k=1}^4 \Gamma^{kk} = \mathbb{I}$ ,  $(\Gamma^{kj})^\dagger = \Gamma^{jk}$ , where  $\mathbb{I}$  is the identity operator in  $\mathcal{H}$ . It is a matter of substitution to verify the expressions  $\rho^2 = \sum_{k,j=1}^4 s_{km} \Gamma^{km}$  and  $s_{km} = \sum_{\ell=1}^4 r_{k\ell} r_{\ell m}$ . Then, using the factorization  $r_{kj} = \alpha_k \alpha_j^*$ , together with the normalization of  $|\psi\rangle$ , we obtain  $\rho^2 = \rho$ . Therefore  $\text{Tr} \rho^2 = 1$ . ■

• The eigenvalues and eigenvectors of  $\rho_X$  discussed in Section 2.1 are given by the expressions

$$\begin{aligned}\Lambda_1 &= \frac{1}{2} \left[ r_{11} + r_{44} + \sqrt{(r_{11} + r_{44})^2 - 4(x_0^2 - x^2)} \right], \\ \Lambda_2 &= \frac{1}{2} \left[ r_{11} + r_{44} - \sqrt{(r_{11} + r_{44})^2 - 4(x_0^2 - x^2)} \right], \\ \Lambda_3 &= \frac{1}{2} \left[ r_{22} + r_{33} + \sqrt{(r_{22} + r_{33})^2 - 4(y_0^2 - y^2)} \right], \\ \Lambda_4 &= \frac{1}{2} \left[ r_{22} + r_{33} - \sqrt{(r_{22} + r_{33})^2 - 4(y_0^2 - y^2)} \right],\end{aligned}\tag{A-1}$$

and

$$\begin{aligned}|\epsilon_1\rangle &= \frac{x e^{i\theta} |e_1\rangle + (\Lambda_1 - r_{11}) |e_4\rangle}{\sqrt{(\Lambda_1 - r_{11})^2 + x^2}}, & |\epsilon_2\rangle &= \frac{x e^{i\theta} |e_1\rangle + (\Lambda_2 - r_{11}) |e_4\rangle}{\sqrt{(\Lambda_2 - r_{11})^2 + x^2}}, \\ |\epsilon_3\rangle &= \frac{y e^{i\phi} |e_2\rangle + (\Lambda_3 - r_{22}) |e_3\rangle}{\sqrt{(\Lambda_3 - r_{22})^2 + y^2}}, & |\epsilon_4\rangle &= \frac{y e^{i\phi} |e_2\rangle + (\Lambda_4 - r_{22}) |e_3\rangle}{\sqrt{(\Lambda_4 - r_{22})^2 + y^2}}.\end{aligned}\tag{A-2}$$

In the above expressions we have used the notation introduced in Section 2.1 for the convex set  $\mathcal{S}$ . Namely,  $x_0 = \sqrt{r_{11} r_{44}}$ ,  $r_{14} = x e^{i\theta}$ , and  $y_0 = \sqrt{r_{22} r_{33}}$ ,  $r_{23} = y e^{i\phi}$ .

• Let us review the situation when the matrix-elements of  $\rho_X$  fulfill Proposition Q. That is, when the X-state is pure. To satisfy (3), given that  $r_{13}$  and  $r_{34}$  have  $\alpha_3$  as a common factor, it will be enough to take  $\alpha_3 = 0$  so that these two matrix-elements are equal to zero. Similarly, we take  $\alpha_2 = 0$  to cancel  $r_{24}$  and  $r_{12}$ . These  $\alpha$ -parameters also give  $r_{22} = r_{33} = 0$ , so the second identity of Eq. (4) is automatically satisfied. Furthermore, we immediately obtain  $r_{23} = 0$ . Then, the X-state (5) is reduced to the projector  $\rho_X = |\psi_{14}\rangle\langle\psi_{14}|$ , with

$$|\psi_{14}\rangle = \alpha_1 |e_1\rangle + \alpha_4 |e_4\rangle, \quad |\alpha_1|^2 + |\alpha_4|^2 = 1.\tag{A-3}$$

If we also demand that the first identity of Eq. (4) holds, then  $|\alpha_1| = |\alpha_4|$  and  $\vec{\lambda}_R = (\frac{1}{2}, \frac{1}{2})$ . After adjusting the phases and requiring orthogonality, from (A-3) we recover the first pair of Bell-states (7). Proceeding in a similar way, now eliminating  $\alpha_1$  and  $\alpha_4$ , we obtain another projector  $\rho_X = |\psi_{23}\rangle\langle\psi_{23}|$ , where

$$|\psi_{23}\rangle = \alpha_2|e_2\rangle + \alpha_3|e_3\rangle, \quad |\alpha_2|^2 + |\alpha_3|^2 = 1. \quad (\text{A-4})$$

In this case, the second identity of Eq. (4) gives  $\vec{\lambda}_L = (\frac{1}{2}, \frac{1}{2})$ , so that (A-4) leads to the second pair of Bell-states (8).

• The convex optimization discussed in Section 3 requires Lagrange multipliers. Consider the function  $f(r_{11}, r_{22}, r_{33}, r_{44}) = \sqrt{r_{11}r_{44}} + \sqrt{r_{22}r_{33}}$ , together with the constraint

$$g(r_{11}, r_{22}, r_{33}, r_{44}) = r_{11} + r_{22} + r_{33} + r_{44} - 1 = 0. \quad (\text{A-5})$$

Using  $m$  as the Lagrange multiplier associated with constraint  $g$ , we have the system

$$\begin{aligned} \frac{\partial f}{\partial r_{11}} - m \frac{\partial g}{\partial r_{11}} &= \frac{r_{44}}{2\sqrt{r_{11}r_{44}}} - m = 0, & \frac{\partial f}{\partial r_{22}} - m \frac{\partial g}{\partial r_{22}} &= \frac{r_{33}}{2\sqrt{r_{22}r_{33}}} - m = 0, \\ \frac{\partial f}{\partial r_{33}} - m \frac{\partial g}{\partial r_{33}} &= \frac{r_{22}}{2\sqrt{r_{22}r_{33}}} - m = 0, & \frac{\partial f}{\partial r_{44}} - m \frac{\partial g}{\partial r_{44}} &= \frac{r_{11}}{2\sqrt{r_{11}r_{44}}} - m = 0. \end{aligned}$$

Therefore

$$m = \frac{r_{11}}{2\sqrt{r_{11}r_{44}}} = \frac{r_{22}}{2\sqrt{r_{22}r_{33}}} = \frac{r_{33}}{2\sqrt{r_{22}r_{33}}} = \frac{r_{44}}{2\sqrt{r_{11}r_{44}}}.$$

The simplest way to satisfy these equalities is by making  $r_{11} = r_{44}$  and  $r_{22} = r_{33}$ . In this case  $f = r_{11} + r_{22}$ . Then, from (A-5) it is found that  $1/2$  is the maximum value we are looking for.

• The rank of states  $\rho_{\mathcal{M}_x}$  that are represented by matrices (17) is as follows

$$\text{rank}(\rho_{\mathcal{M}_x})|_{y_0=0} = \begin{cases} 3, & r_{22} = 0 \text{ or } r_{33} = 0 \\ 2, & r_{22} = 0 \text{ and } x = x_0 \\ 2, & r_{33} = 0 \text{ and } x = x_0 \\ 2, & r_{22} = r_{33} = 0 \\ 1, & r_{22} = r_{33} = 0 \text{ and } x = x_0 \end{cases} \quad (\text{A-6})$$

In turn, the rank of states  $\rho_{\mathcal{M}_y}$  that are represented by matrices (18) reads

$$\text{rank}(\rho_{\mathcal{M}_y})|_{x_0=0} = \begin{cases} 3, & r_{11} = 0 \text{ or } r_{44} = 0 \\ 2, & r_{11} = 0 \text{ and } y = y_0 \\ 2, & r_{44} = 0 \text{ and } y = y_0 \\ 2, & r_{11} = r_{44} = 0 \\ 1, & r_{11} = r_{44} = 0 \text{ and } y = y_0 \end{cases} \quad (\text{A-7})$$

## Author Contributions

Conceptualization O.R.-O.; methodology, formal analysis, investigation, original draft preparation and review, S.L.-H., C.Q. and O.R.-O.; editing, project administration and funding acquisition, O.R.-O. All authors have read and agreed to the published version of the manuscript.

## Funding

This research was funded by Consejo Nacional de Humanidades, Ciencia y Tecnología (CONACHyT, Mexico), grant number A1-S-24569, and by Instituto Politécnico Nacional (IPN, Mexico), project SIP20242277.

## Acknowledgment

S.L.-H acknowledges the support from CONAHCyT through the scholarship 592045.

## References

- [1] M.A. Nielsen and I.L. Chuang, *Quantum Computation and Quantum Information*, Cambridge University Press, Cambridge, United Kingdom, 2000
- [2] A. Einstein, B. Podolsky and N. Rosen, Can Quantum-Mechanical Description of Physical Reality Be Considered Complete?, *Phys. Rev.* **47** (1935) 777
- [3] E. Schrödinger, Die gegenwärtige Situation in der Quantenmechanik, *Die Naturwissenschaften* **23** (1935) 807
- [4] J.S. Bell, On the Einstein Podolsky Rosen Paradox, *Physics* **1** (1964) 195
- [5] A. Aspect, P. Grangier and G. Roger, Experimental Tests of Realistic Local Theories via Bell's Theorem, *Phys. Rev. Lett.* **47** (1981) 460
- [6] O. Rosas-Ortiz, Beyond the dynamical universe. Unifying block universe physics and time as experienced, *Contemp. Phys.* **60** (2019) 188
- [7] V. Vedral, M.B. Plenio, M.A. Rippin and P.L. Knight, Quantifying Entanglement, *Phys. Rev. Lett.* **78** (1997) 2275
- [8] M. Horodecki, Entanglement Measures, *Quantum Inf. Comput.* **1** (2001) 3
- [9] R. Horodecki, P. Horodecki. M. Horodecki and K. Horodecki, Quantum entanglement, *Rev. Mod. Phys.* **81** (2009) 865
- [10] O. Gühne and G. Tóth, Entanglement detection, *Phys. Rep.* **474** (2009) 1
- [11] M. Plenio and S.S. Virmani, An Introduction to Entanglement Theory, in Andersson, E., Öhberg, P. (eds), *Quantum Information and Coherence*, Scottish Graduate Series, Springer, Cham, 2014
- [12] S. Luna-Hernández, Genuine multipartite entanglement in three-qubit *XYZ* Heisenberg systems, *J. Phys.: Conf. Ser.* **2667** (2023) 012034

- [13] S. Luna-Hernández, M. Enríquez and O. Rosas-Ortiz, A geometric formulation to measure global and genuine entanglement in three-qubit systems, arXiv:2405.09466
- [14] A. Peres, Separability criterion for density matrices, *Phys. Rev. Lett.* **77** (1996) 1413
- [15] M. Horodecki, P. Horodecki and R. Horodecki, Separability of mixed states: necessary and sufficient conditions, *Phys. Lett. A* **223** (1996) 1
- [16] R.F. Werner, Quantum states with Einstein-Podolsky-Rosen correlations admitting a hidden-variable model, *Phys. Rev. A* **40** (1989) 4277
- [17] J. Lee and M.S. Kim, Entanglement Teleportation via Werner States, *Phys. Rev. Lett.* **84** (2000) 4236
- [18] T. Hiroshima and S. Ishizaka, Local and nonlocal properties of Werner states, *Phys. Rev. A* **62** (2000) 044302
- [19] A.O. Pittenger and M.H. Rubin, Note on separability of the Werner states in arbitrary dimensions, *Opt. Commun.* **179** (2000) 447
- [20] D.W. Lyons, A.M. Skelton and S.N. Walck, Werner State Structure and Entanglement Classification, *Adv. Math. Phys.* (2012) 463610
- [21] S. Díaz-Solórzano and E. Castro, Exact analytical solution of Entanglement of Formation and Quantum Discord for Werner state and Generalized Werner-Like states, arXiv:1802.05877v1 [quant-ph]
- [22] Y. Zhang and E. Chitambar, Exact Steering Bound for Two-Qubit Werner States, *Phys. Rev. Lett.* **132** (2024) 250201
- [23] D. Jiang, C. Zhai, Y. Song, et al, Generating Bell states and Werner states of two qubits via optical field, *Phys. Scripta.* **99** (2024) 055109
- [24] W.J. Munro, D.F.V. James, A.G. White, and P.G. Kwiat, Maximizing the entanglement of two mixed qubits, *Phys. Rev. A* **64** (2001) 030302(R)
- [25] N. Quesada, A. Al-Qasimi and D.F.V. James, Quantum properties and dynamics of X states, *J. Mod. Phys.* **59** (2012) 1322
- [26] P.E.M.F. Mendonca, M.A. Marchioli and D. Galetti, Entanglement universality of two-qubit X-states, *Ann. Phys.* **351** (2014) 79
- [27] M. Aulbach, D. Markham and M. Muraó, The maximally entangled symmetric state in terms of the geometric measure, *N. J. Phys.* **12** (2010) 073025
- [28] S. Hill and W.K. Wootters, Entanglement of a pair of quantum bits, *Phys. Rev. Lett.* **78** (1997) 5022
- [29] W.K. Wootters, Entanglement of formation for any arbitrary state of two qubits, *Phys. Rev. Lett.* **80** (1998) 2245

- [30] M. Gessner, E. Laine, H. Breuer, and J. Piilo, Correlations in quantum states and the local creation of quantum discord, *Phys. Rev. A* **85** (2012) 052122
- [31] L. Wang, J.H. Huang, J.P. Dowling, and S.Y. Zhu, Quantum information transmission, *Quantum Inf. Process.* **12** (2013) 899
- [32] A. Mani, V. Karimipour, and L. Memarzadeh, Comparison of parallel and antiparallel two-qubit mixed states, *Phys. Rev. A* **91** (2015) 012304
- [33] S. Nag, A. Lahiri and G. Ghosh, Entropy production due to coupling to a heat bath in the kicked rotor problem, *Phys. Lett. A* **292** (2001) 43
- [34] D.S. Bernstein, *Matrix Mathematics: Theory, Facts and Formulas*, 2nd Edition, Princeton University Press, 2009
- [35] C.H. Bennett, D.P. DiVincenzo, J. Smolin, and W.K. Wootters, *Phys. Rev. A* **54** (1996) 3824
- [36] M. Enríquez, C. Quintana and O. Rosas-Ortiz, Time-evolution of entangled bipartite atomic systems in quantized radiation fields, *J. Phys.: Conf. Ser.* **512** (2014) 012022
- [37] C. Quintana and O. Rosas-Ortiz, Note on the quantum correlations of two qubits coupled to photon baths, *J. Phys.: Conf. Ser.* **624** (2015) 012004
- [38] C. Quintana, Additional quantum properties of entangled bi-partite qubit systems coupled to photon baths, *J. Phys.: Conf. Ser.* **698** (2016) 012022
- [39] D. J. Fernández C. and O. Rosas-Ortiz, Inverse techniques and evolution of spin-1/2 systems, *Phys. Lett. A* **236** (1997) 275
- [40] M. Enríquez and O. Rosas-Ortiz, The Kronecker product in terms of Hubbard operators and the Clebsch-Gordan decomposition of  $SU(2) \times SU(2)$ , *Ann. Phys.* **339** (2013) 218